Transcom 3 inversion intercomparison: Model mean results for the estimation of seasonal carbon sources and sinks

Kevin Robert Gurney, Rachel M. Law, A. Scott Denning, Peter J. Rayner, Bernard C. Pak, David Baker, Philippe Bousquet, Lori Bruhwiler, Yu-Han Chen, Philippe Ciais, et al.

Transcom 3 inversion intercomparison: Model mean results for the estimation of seasonal carbon sources and sinks

Kevin Robert Gurney,[1] Rachel M. Law,[2] A. Scott Denning,[1] Peter J. Rayner,[2] Bernard C. Pak,[3] David Baker,[4] Philippe Bousquet,[5] Lori Bruhwiler,[6] Yu-Han Chen,[7] Philippe Ciais,[5] Inez Y. Fung,[8] Martin Heimann,[9] Jasmin John,[8] Takashi Maki,[10] Shamil Maksyutov,[11] Philippe Peylin,[5] Michael Prather,[3] and Shoichi Taguchi[12]

Received 16 June 2003; revised 24 October 2003; accepted 19 November 2003; published 24 January 2004.

[1] The TransCom 3 experiment was begun to explore the estimation of carbon sources and sinks via the inversion of simulated tracer transport. We build upon previous TransCom work by presenting the seasonal inverse results which provide estimates of carbon flux for 11 land and 11 ocean regions using 12 atmospheric transport models. The monthly fluxes represent the mean seasonal cycle for the 1992 to 1996 time period. The spread among the model results is larger than the average of their estimated flux uncertainty in the northern extratropics and vice versa in the tropical regions. In the northern land regions, the model spread is largest during the growing season. Compared to a seasonally balanced biosphere prior flux generated by the CASA model, we find significant changes to the carbon exchange in the European region with greater growing season net uptake which persists into the fall months. Both Boreal North America and Boreal Asia show lessened net uptake at the onset of the growing season with Boreal Asia also exhibiting greater peak growing season net uptake. Temperate Asia shows a dramatic springward shift in the peak timing of growing season net uptake relative to the neutral CASA flux while Temperate North America exhibits a broad flattening of the seasonal cycle. In most of the ocean regions, the inverse fluxes exhibit much greater seasonality than that implied by the ΔpCO_2 derived fluxes though this may be due, in part, to misallocation of adjacent land flux. In the Southern Ocean, the austral spring and fall exhibits much less carbon uptake than implied by ΔpCO_2 derived fluxes. Sensitivity testing indicates that the inverse estimates are not overly influenced by the prior flux choices. Considerable agreement exists between the model mean, annual mean results of this study and that of the previously published TransCom annual mean inversion. The differences that do exist are in poorly constrained regions and tend to exhibit compensatory fluxes in order to match the global mass constraint. The differences between the estimated fluxes and the prior model over the northern land regions could be due to the prior model respiration response to temperature. Significant phase differences, such as that in the Temperate Asia region, may be due to the limited observations for that region. Finally, differences in the boreal land regions between the prior model and the estimated fluxes may be a reflection of the timing of spring thaw and an imbalance in respiration versus photosynthesis. *INDEX TERMS:* 0322 Atmospheric Composition and Structure: Constituent sources and sinks; 1615 Global Change: Biogeochemical processes (4805); 0315 Atmospheric Composition and Structure: Biosphere/atmosphere interactions; *KEYWORDS:* carbon transport, inversion

[1]Department of Atmospheric Science, Colorado State University, Fort Collins, Colorado, USA.
[2]CSIRO Atmospheric Research, Aspendale, Victoria, Australia.
[3]Earth System Science, University of California, Irvine, Irvine, California, USA.
[4]National Center for Atmospheric Research, Boulder, Colorado, USA.
[5]Laboratoire des Sciences du Climate et de l'Environment, Gif-sur-Yvette, France.
[6]Climate Monitoring and Diagnostics Laboratory, NOAA, Boulder, Colorado, USA.
[7]Department of Earth, Atmospheric, and Planetary Science, Massachusetts Institute of Technology, Cambridge, Massachusetts, USA.
[8]Center for Atmospheric Sciences, University of California, Berkeley, Berkeley, California, USA.
[9]Max-Planck-Institute fur Biogeochemie, Jena, Germany.
[10]Quality Assurance Section, Atmospheric Environment Division, Observations Department, Japan Meteorological Agency, Tokyo, Japan.
[11]Institute for Global Change Research, Frontier Research System for Global Change, Yokohama, Japan.
[12]National Institute of Advanced Industrial Science and Technology, Ibaraki, Japan.

0886-6236/04/2003GB002111

Citation: Gurney, K. R., et al. (2004), Transcom 3 inversion intercomparison: Model mean results for the estimation of seasonal carbon sources and sinks, *Global Biogeochem. Cycles*, *18*, GB1010, doi:10.1029/2003GB002111.

1. Introduction

[2] The spatial and temporal pattern of atmospheric CO_2 can be used to infer sources and sinks of carbon through the inversion of atmospheric tracer transport. A quantitative understanding of sources and sinks in both space and time is an essential ingredient to reliably predicting future levels of atmospheric CO_2. The use of the inversion technique has been employed at a variety of temporal and spatial scales. With the increase in spatial coverage of CO_2 observations and the development of 3D tracer transport models, recent inversions have been performed at the continental scale and have explored both the seasonal cycle of carbon sources and sinks and their interannual variability [*Enting et al.*, 1995; *Fan et al.*, 1998; *Rayner et al.*, 1999; *Bousquet et al.*, 1999, 2000; *Baker*, 2001; *Gurney et al.*, 2002; *Peylin et al.*, 2002; *Gurney et al.*, 2003]. Further reductions in spatial scale have been attempted through the use of adjoint transport models though the current global CO_2 observational network poses a constraint on the reliability of fluxes estimated at subcontinental scales [*Kaminski et al.*, 1999; *Rödenbeck et al.*, 2003].

[3] Estimates of continental carbon sources and sinks in the last decade have shown considerable disagreement. Though many aspects of these studies share common elements, different tracer transport models were often used. The primary goal of the TransCom 3 experiment was to assess the contribution of tracer transport to the spread of atmospheric CO_2 inverse results and builds on the earlier TransCom work [*Law et al.*, 1996; *Denning et al.*, 1999]. The experiment can also test other sensitivities in the inversion process (e.g., inversion set-up, observational data choices) since more reliable results are expected by examining sensitivities with a range of transport models than with just one or two.

[4] TransCom 3 was designed to estimate carbon sources and sinks at annual, seasonal, and interannual timescales. Annual mean results have already been published elsewhere and have reported on the model mean results of the control or "base case" inversion, the sensitivity of this control case to inversion set-up/observational network choices, and model-to-model differences [*Gurney et al.*, 2002, 2003; *Law et al.*, 2003]. Analysis of the interannual results are currently underway.

[5] Here we present an average seasonal inversion result. In this experiment, we estimate fluxes for each month of an average year determined as the mean of the 1992 to 1996 period. Section 2 provides a description of the methods employed including the choices involved in creating the control inversion set-up. Section 3 presents the model mean results of the control inversion including sensitivity to aspects of the inversion set-up. Section 4 contrasts the current results to the annual mean control inversion and discusses possible mechanisms responsible for the estimated regional fluxes. This paper focuses on the model average results. Future work will explore the model-to-model differences. While the model average is not presented as the mean of a randomly varying statistical ensemble, it does represent a compact representation of the tendencies inherent in the majority of models used in inverse work in recent years. It is important to note that individual model estimates cannot be judged by their proximity to the model mean.

2. Methods

[6] The inversion approach used in this study follows the Bayesian synthesis method [*Tarantola*, 1987; *Enting*, 2002] A detailed description of the formalism employed and references to source material is given in previous work for the annual mean TransCom inversion [*Gurney et al.*, 2003]. The method used here is the same except that monthly mean CO_2 observations are used rather than the annual mean values.

[7] Because results from a group of transport models will be presented, two different measures of uncertainty will be computed in the present work. The RMS of the individual model flux uncertainties can be calculated as

$$\overline{\mathbf{C}\left(\vec{S}\right)} = \sqrt{\sum_{n=1}^{N_{\text{models}}} \left(\mathbf{C}\left(\vec{S}\right)_n\right)^2 \Big/ N_{\text{models}}}, \tag{1}$$

where S is a model flux estimate and $\boldsymbol{C}\,(S)_n$ represents the monthly posterior uncertainty estimates for each model. We designate this mean uncertainty the "within-model" uncertainty. The spread of flux estimates across models is represented by the standard deviation,

$$\sigma\left(\vec{S}\right) = \sqrt{\sum_{n=1}^{N_{\text{models}}} \left(\vec{S} - \overline{\left(\vec{S}\right)}_n\right)^2 \Big/ N_{\text{models}}}, \tag{2}$$

and designated the "between-model" uncertainty. Unless specifically noted, all uncertainties quoted in the text represent the total uncertainty which are the within- and between-model combined in quadrature.

2.1. Experimental Design

2.1.1. Forward Simulations

[8] Twelve transport models (or model variants) ran a series of forward CO_2 tracer simulations [*Gurney et al.*, 2000] in order to construct model-specific response functions used to perform the inversion for seasonal carbon sources and sinks. Though monthly fluxes are resolved in the current study, the same 12 transport models were also included in an annual mean inversion and are described in detail in previous work [*Gurney et al.*, 2003].

[9] For the seasonal experiment presented here, the forward simulations were run as greens functions. A total of 268 tracers were simulated by each model, four of which were "background" global fluxes and 264 of which were region/month fluxes representing a combination of

12 months and the 22 land and ocean regions described in the annual mean inversion experiment [*Gurney et al.*, 2002]. The background fluxes were emitted for a single year, then discontinued, allowing the CO_2 concentration field to decay for the following 2 years of simulation. The region/month flux combinations were emitted for a single month then discontinued for the remainder of the 3-year simulation. These responses were converted to a single 12-month stationary response by compositing like months (summing all Januaries, all Februaries, etc., in the 3-year span) and detrending (removing the concentration trend resulting from the constant emissions in the forward simulations).

[10] The four background fluxes consisted of 1990 and 1995 fossil fuel emission fields, an annually balanced, seasonal biosphere exchange and air-sea gas exchange [*Andres et al.*, 1996; *Randerson et al.*, 1997; *Takahashi et al.*, 1999; A. L. Brenkert, Carbon dioxide emission estimates from fossil-fuel burning, hydraulic cement production, and gas flaring for 1995 on a one degree grid cell basis, available at http://cdiac.esd.ornl.gov/ndps/ndp058a.html]. These fluxes are included in the inversion with a small prior uncertainty so that their magnitude is effectively fixed. The 264 region/month fluxes estimated by the inversion are deviations from these global background fluxes for each month in a climatological year. The background fossil fuel emission fluxes were prescribed without seasonality. The neutral terrestrial fluxes were purely seasonal, and the background ocean fluxes were prescribed with both seasonal variations and annual mean uptake.

[11] Further details and references for the forward fluxes are given by *Gurney et al.* [2002]. Full details of the experimental protocol are presented by *Gurney et al.* [2000].

2.1.2. Inversion Set-Up and Observational Data

[12] Prior estimates of the fluxes in each of the 264 region/month flux combinations were determined from independent estimates of terrestrial and oceanic exchange. The land region prior flux estimates incorporate results from recent inventory studies and are identical to the annual mean values used in the annual mean inversion [*Gurney et al.*, 2003]. Where more than one estimate for a given region was considered, a midpoint of the estimate spread was used. Because the land region prior fluxes are only available as annual mean values, these were distributed evenly over those months considered the most likely to capture the emission or uptake implied by the prior flux. The ocean region prior flux estimates were prescribed as zero for each month.

[13] The prior flux uncertainty is important for keeping the estimated fluxes within biogeochemically realistic bounds. For land regions in a given month, we chose the combination of the uncertainties employed in our annual mean control case [*Gurney et al.*, 2002], and 30% each of NPP and respiration provided by the CASA model of net ecosystem production [*Randerson et al.*, 1997]. Since it is unlikely that a given region/month flux adjustment would exceed these values, this provides a reasonable, ecologically relevant upper bound. The prior ocean uncertainties were twice the annual mean uncertainty values used in the annual mean control inversion.

[14] We invert 5-year (1992–1996) mean measurements for each month at 75 sites taken from the GLOBALVIEW-2000 data set [*GLOBALVIEW-CO2*, 2000]. GLOBALVIEW is a data product that interpolates CO_2 measurements to a common time interval. Gaps in the data are filled by extrapolation from marine boundary layer measurements. Sites were chosen where the extrapolated data accounts for less than 30% of the 1992–1996 period. This station set is identical to that used in the annual mean inversion published previously except in the current experiment, the station in Darwin, Australia, was removed due to recent work showing Darwin as unrepresentative of the region [*Law et al.*, 2003]. The uncertainty attached to each data value, *C(D)*, was derived from the monthly residual standard deviation (RSD) of individual observations around a smoothed time series as given by GLOBALVIEW. This choice was based on the assumption that the distribution of RSD (higher RSD values for northern and continental sites and lower RSD values for Southern Hemisphere oceanic sites) reflects the high-frequency variations in transport and regional flux that large-scale transport models are unable to accurately simulate. *GLOBALVIEW-CO2* [2000] provides monthly RSD values averaged over 1979–1996 and annual RSD values for each separate year. To obtain monthly values for 1992–1996, we scale the 1979–1996 monthly values by the ratio of the 1992–1996 mean annual RSD to the 1979–1996 mean annual RSD.

[15] Direct use of the RSD values for the data uncertainty results in a total reduced χ^2 that is much smaller than unity [*Tarantola*, 1987, p. 212]. This indicates that the predicted concentrations fit the data much better than the uncertainty assigned to the data itself and that the uncertainty should be reduced. The aim is to scale the RSD such that the inversion produces a total χ^2 of 1.0. When making this adjustment, we limit the reduction such that the minimum uncertainty at any site is equivalent to 0.25 ppm on the annual mean concentration and we also adjust the uncertainty for data records that are co-located. The details are as follows: the RSD was divided by $(3.6*P)^{0.5}$ where P is the proportion of real data in the record and 3.6 is chosen to satisfy our total χ^2 criteria. These monthly uncertainties were converted to equivalent annual uncertainties with the following expression:

$$\sigma_a = \frac{\sqrt{\sum_{m=1}^{12} \sigma_m^2}}{A}, \tag{3}$$

where σ_a is the equivalent annual uncertainty, σ_m is the monthly uncertainty, and A represents the autocorrelation timescale for the specific station (typically around 4 months). If the annualized uncertainty was less than the minimum uncertainty used in the annual mean control inversion of 0.25 ppm, the monthly uncertainty values were increased to an uncertainty given by

$$\sigma_m^{\min} = 0.25*\sqrt{A}. \tag{4}$$

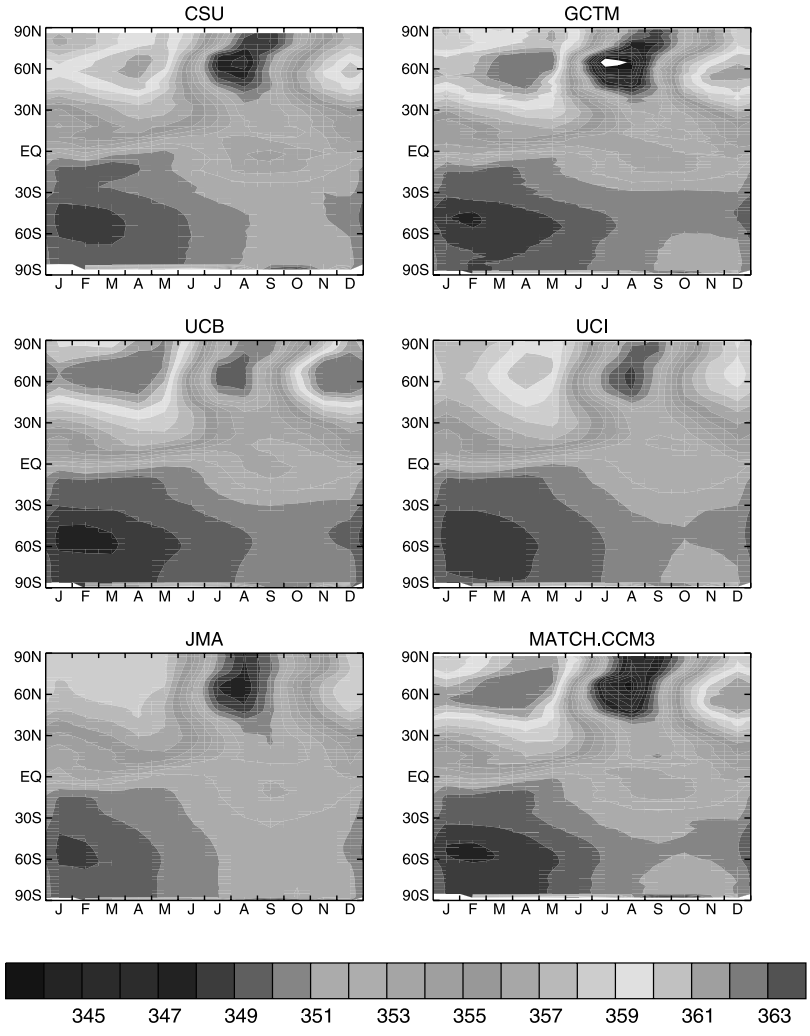

Figure 1. Zonal mean monthly predicted concentration driven by the background fluxes (fossil fuel, seasonally balanced biosphere exchange, ocean exchange) for each of the participating tracer transport models. See color version of this figure at back of this issue.

Finally, the uncertainty was increased for those sites that are likely to occur in the same model grid-cell. These adjustments gave values ranging from 0.17 ppm for a given month at remote, ''clean air'' sites to 4.8 ppm for continental, ''noisy'' sites and a mean total χ^2 averaged across the models of 1.0.

3. Results

3.1. Background Simulation Results

[16] The forward simulations of the four background fluxes provide a measure of model-to-model transport differences. Figure 1 shows the zonal mean seasonality of the model response to the background fluxes at the surface. The seasonality for each of the models reflect both the seasonality in the surface forcing and transport.

[17] A strong seasonal response is evident in the Northern Hemisphere for the MATCH variants, NIES, NIRE, and TM3 while CSU, JMA, UCI, and TM2 exhibit weak northern seasonality. The response of the GCTM model shows a winter maximum that places it in the middle of the participating models but exhibits a strong summer concentration minimum.

[18] The spatial extent of the maxima is also variable among the models. Of those models with a pronounced seasonal response, MATCH:NCEP and NIES show winter maxima that stretch almost evenly from 45°N to the pole whereas the other strongly seasonal models exhibit less extensive winter maxima.

[19] Though the full latitudinal distribution of the background simulation provides a useful overview of the different model responses, the inversion results are driven by CO_2 observations at the stations only. Figure 2 shows the simulated background seasonal amplitude at stations north of 35°N latitude plotted against the observed seasonal amplitude. In this figure, the seasonal amplitude is defined as the background response difference between the average of October through March (maximum) and the average of June through August (minimum) at the stations. The figure also provides the average amplitude value across all the stations north of 35°N for each of the models and a one-to-one line.

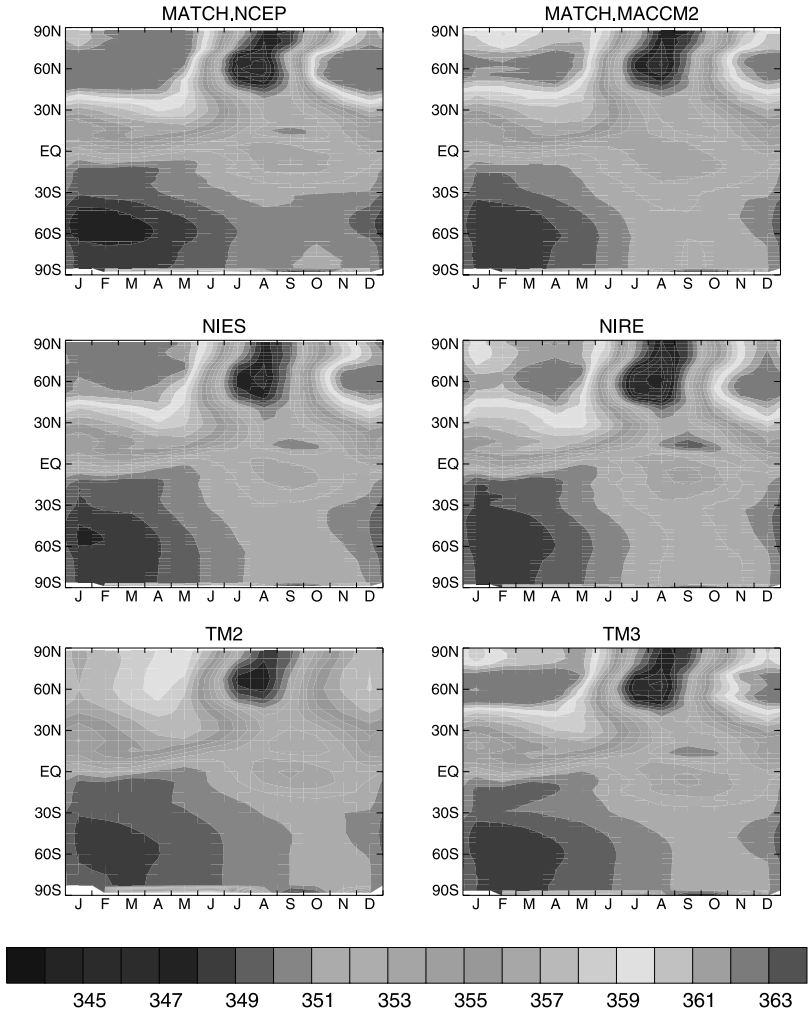

Figure 1. (continued)

[20] Consistent with Figure 1, some of the models exhibit weak northern seasonality (CSU, TM2, UCI, and JMA) while others produce greater seasonality (NIRE, NIES, and M:NCEP). This spread in model behavior has been previously noted for both biosphere CO_2 and the SF_6 tracer and tends to relate to the vigor of vertical transport [*Gurney et al.*, 2003; *Denning et al.*, 1999]. Both the magnitude and the model spread evident in the seasonal response to the background fluxes are dominated by the background biosphere exchange. Through the inversion process, in which mismatches between the background response and the observed concentration are minimized (modulated by the station uncertainty), models that underestimate the background seasonality must construct sources and sinks in order to amplify the seasonal exchange with the surface and vice versa.

[21] Previous TransCom work with a different neutral biosphere exchange and a somewhat different group of tracer transport models showed consistent overestimation of the seasonal amplitude in the Northern Hemisphere [*Law et al.*, 1996, Figure 10]. Since the biospheric exchange dominates the seasonality of the background flux, this suggests that the current CASA neutral biosphere fluxes are much more consistent with the CO_2 observations than fluxes used in the past.

3.2. Inversion Results

3.2.1. Model Mean Results

[22] Figure 3 shows the control case estimated seasonal fluxes, prior fluxes, and uncertainties for the ocean and land regions combined into north, tropical, and south aggregates. The estimated fluxes do not include fossil fuel and represent the average across the 12 models.

[23] Two measures of uncertainty are presented in Figure 3 (see section 2). For any region, the ''within uncertainty'' (distance from posterior flux to circles) must be smaller than the prior flux uncertainty (distance from prior flux to heavy dashed lines). The magnitude of the decrease indicates the degree to which the final flux estimate is constrained by the measurements. The northern extratropics and the southern extratropical oceans exhibit the greatest reduction in uncertainty due to the greater number of observing sites and sites with relatively small data uncertainty.

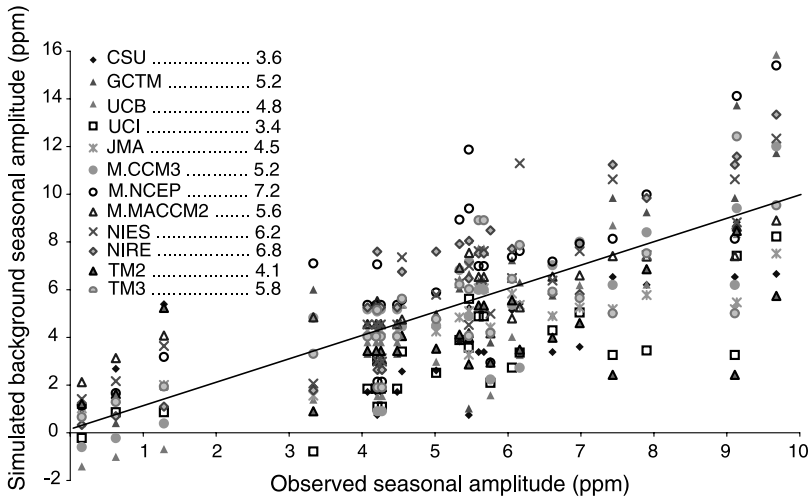

Figure 2. Simulated background seasonal amplitude versus the observed amplitude at stations north of 35°N. Amplitude is defined as the mean October–March concentration minus the mean June–August concentration. The station average simulated values are provided in the legend. The observed station average is 5.6 ppm. A one-to-one line is included. See color version of this figure at back of this issue.

[24] The "between uncertainty" (error bars) indicates the degree to which transport model differences contribute to the range of flux estimates. On land, between uncertainties are largest in the tropical region. The ocean regions exhibit between uncertainties that are largest over the tropics and southern latitudes. The uncertainty also varies over the course of the year. For example, the northern land region exhibits the largest between uncertainty during the northern growing season.

[25] The relative magnitude of these two uncertainty measures provides a reflection of the extent to which the flux estimates are limited by uncertainty associated with the observational data versus the uncertainty associated with transport differences. As can be seen in Figure 3, the northern extratropical regions where more observing stations are available show between uncertainty values that are larger than the within values. In those regions where observations are limited, such as the tropical regions and the southern land regions, the opposite occurs. In some regions such as the southern extratropical oceans, the dominance of simple advective flow and the relative availability of observations with small variability combine to provide between and within uncertainties that are of similar magnitude and represent a significant reduction of uncertainty from the prior.

[26] In the Northern Hemisphere land region, the estimated fluxes in Figure 3 show less emission during March, April, and September and greater uptake during July relative to the prior flux. Significant monthly departures from the prior oceanic flux occur in all of the aggregated ocean regions showing greater seasonality in all instances. However, the correlation (0.66) in the estimated seasonality between the ocean and land for the northern latitudes suggests the possibility that some of the land seasonality is being misallocated to the neighboring ocean region. This is further explored in section 3.2.2 where the sensitivity to prior uncertainties is tested.

[27] Disaggregation of the land regions is shown in Figure 4. Tropical and Southern America are not shown as very few significant departures from the prior flux occur in any months. In addition to the total prior flux shown in Figure 4 for each of the land regions, the portion of the prior flux associated with the neutral biosphere exchange is shown. The difference between these two priors is the flux derived from inventory studies as discussed in section 2.1.2.

[28] In Boreal North America there are deviations outside of the uncertainty range from the prior model in April, June, and August. The departures in June and August suggest a phase shift in the growing season with the estimated uptake occurring later in the year. Model spread is largest in the summer months and is primarily due to discrepancy among the models concerning the timing of the maximum seasonal uptake.

[29] Europe shows significant deviations from the peak of the growing season in June through September with greater net uptake during these months. This increased net uptake relative to the prior is exhibited by every model.

[30] Boreal Asia shows results similar to the boreal region of North America. Small but significant adjustments to the prior flux occurs in March and April indicating a reduction in early spring emissions. Less net uptake is indicated in June and more net uptake is indicated in July. In Temperate North America, the estimated fluxes exhibit a lessened seasonal amplitude relative to the prior estimates with significant deviations occurring in spring and late fall months.

[31] Temperate Asia exhibits a large deviation from the prior flux in the month of June with model mean uptake estimated at -5.1 ± 2.6 Gt C/year as opposed to -1.2 Gt C/year for the prior estimate. As a result, the overall timing of the summer uptake maximum is shifted (June/July) toward the spring relative to the prior seasonality (August). This could be due to an error in the timing of the prior seasonality (CASA model output) or a real

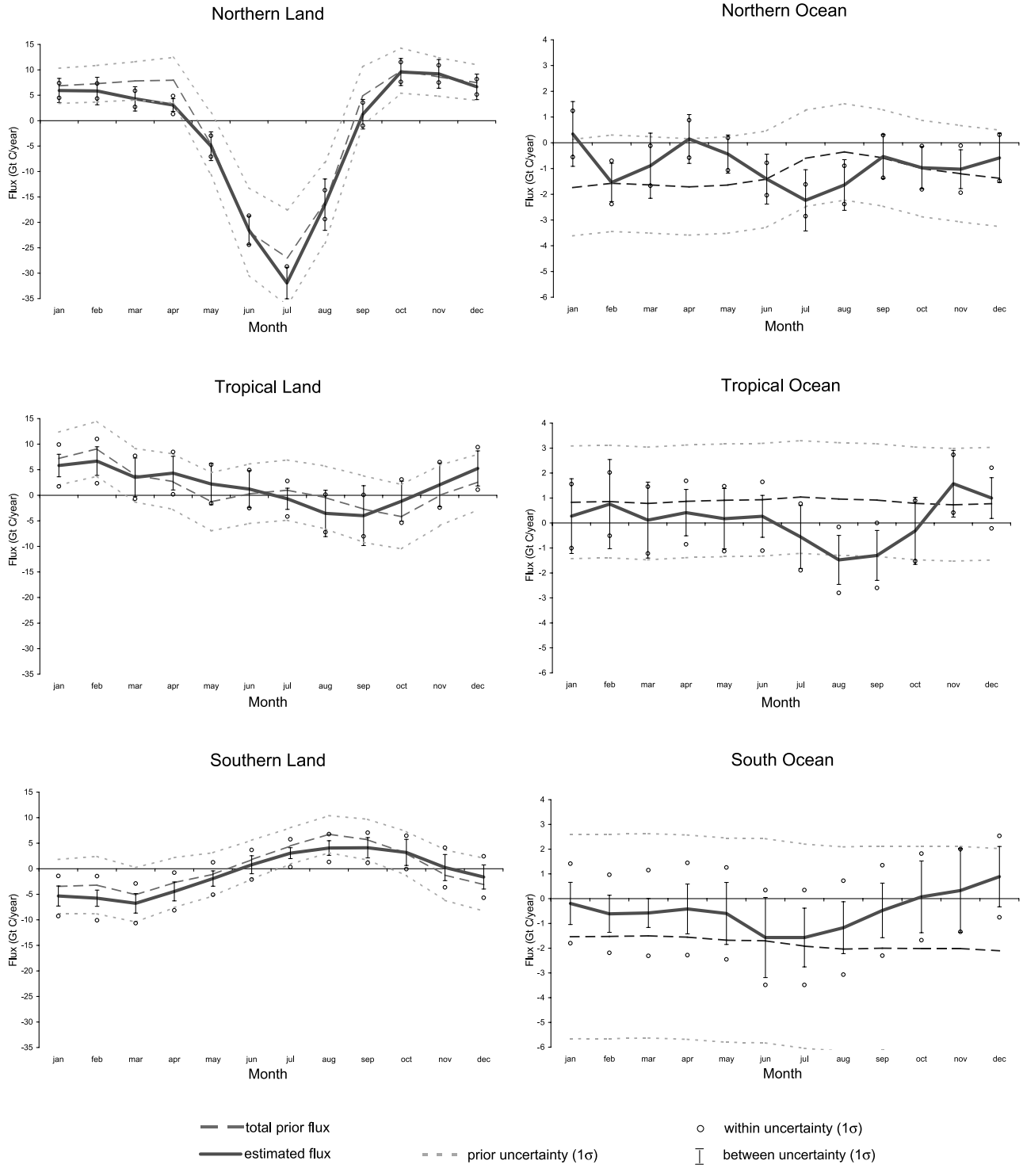

Figure 3. Model mean estimated flux, prior flux, prior uncertainties, and posterior uncertainties for aggregated land and ocean regions. The fluxes do not include fossil fuel emissions. Different scales are used for the land and ocean regions.

advance of net uptake in the 1992 to 1996 time period (assuming the prior model was correctly capturing the long-term seasonality of this region). Only M:MACCM2 places the maximum net uptake in August although July has nearly the same level of net uptake. The two African land regions and Tropical Asia show some significant departures from the prior flux but due to a lack of observational constraint the flux estimates are unreliable. Australasia exhibits departures from the prior estimate in the austral fall changing from a net source to a net sink in April.

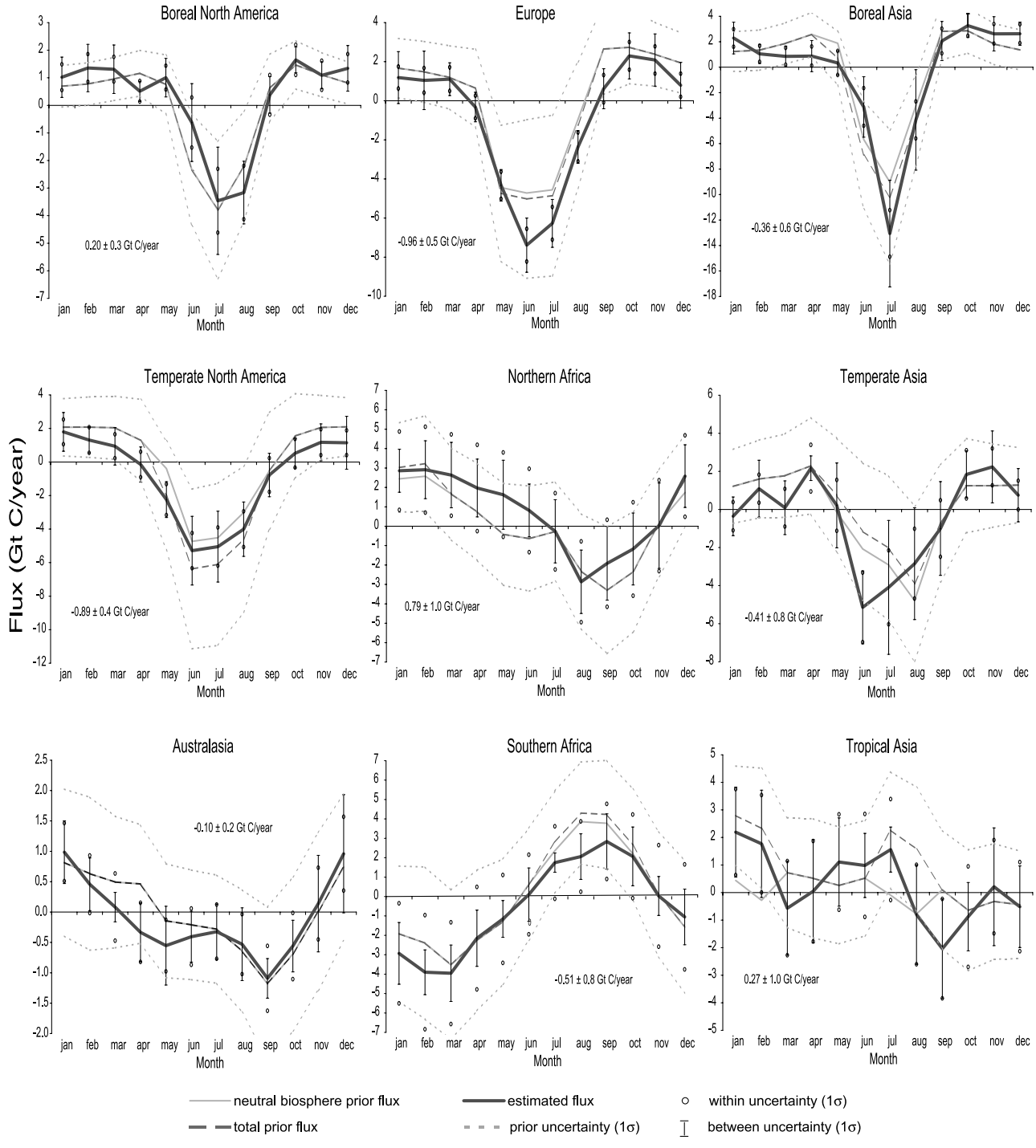

Figure 4. Model mean estimated flux, total prior flux, neutral biosphere prior flux, prior uncertainties, and posterior uncertainties for selected land regions. Numerical estimate of annual mean flux and total uncertainty is provided in each figure. Note that the vertical scale varies. The fluxes do not include fossil fuel emissions.

[32] Disaggregation of selected ocean regions is shown in Figure 5. In many cases, greater seasonality in ocean exchange is implied in the inverse results than was present in the prior ocean flux.

[33] All of the northern ocean regions exhibit heightened seasonality with both the North Pacific and the North Atlantic showing seasonality that is somewhat out of phase with the prior ocean exchange. As mentioned in the discussion of Figure 3, the estimated seasonality has similarities to the adjacent terrestrial seasonal cycle and may be an indication that terrestrial flux is being incorrectly allocated to neighboring ocean regions. In the case of the Southern

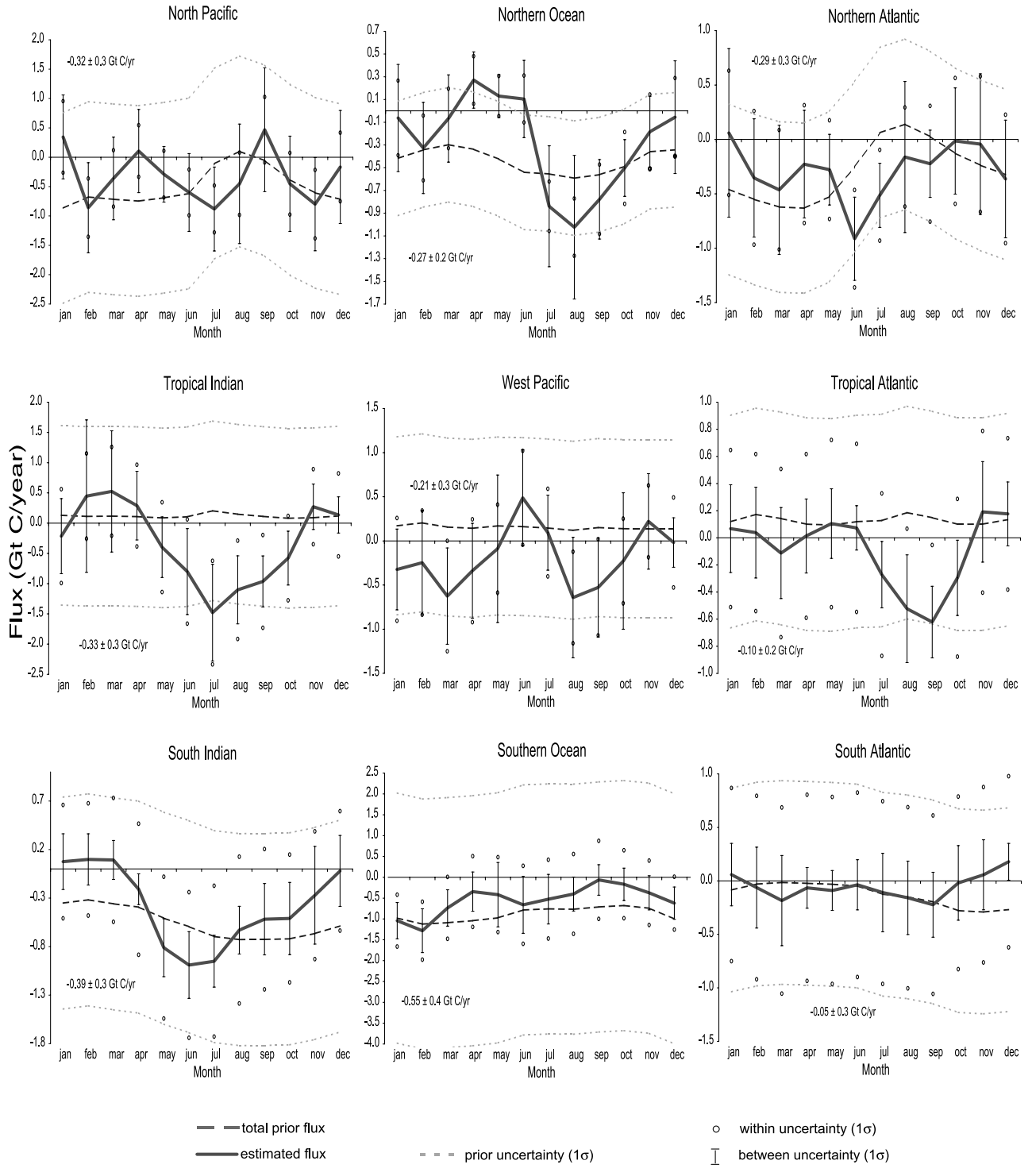

Figure 5. Model mean estimated flux, total prior flux, prior uncertainties, and posterior uncertainties for selected ocean regions. Numerical estimate of annual mean flux and total uncertainty is provided in each figure. Note that the vertical scale varies. The fluxes do not include fossil fuel emissions.

Ocean region, the fall and spring exchange estimated here suggests less uptake than the prior flux. This may explain the discrepancy between the annual mean estimates of ocean flux derived from ΔpCO_2 measurements and those estimated with the inverse estimate [*Gurney et al.*, 2002]. The greatest differences between the prior and estimated flux occur during the austral fall and spring months. Ocean CO_2 measurements are typically only taken during the summer months. Recent ocean measurements taken during January and August 2000 in the Indian Antarctic sector of

the Southern Ocean support this hypothesis. These measurements showed seasonal variations in pCO_2 values south of 50°S that indicate CO_2 uptake in summer and emission in winter [*Metzl et al.*, 2001]. Furthermore, a 1D biogeochemical simulation performed in the same study for all months in the year 2000 showed a seasonality similar to that found here. If the seasonality exhibited in this work is true for other parts of the Southern Ocean, this would reduce the Southern Ocean ΔpCO_2-based uptake estimate, which is currently determined predominantly by summer measurements.

[34] All the tropical ocean regions shown in Figure 5 exhibit greater uptake during the July to September months compared to the prior flux estimate. A small annual mean net uptake is estimated in these ocean regions in contrast to the small annual mean sources of the prior flux estimate. In the case of the tropical Indian Ocean, the annual mean uptake is driven by the Seychelles observations. Removal of this station from the inversion changes this region from an annual mean net sink to an annual mean net source (+0.7 ± 0.4 Gt C/year). The total annual mean tropical ocean flux is estimated as approximately neutral due to the greater net emission from the East Pacific region (0.66 ± 0.3 Gt C/year).

[35] In both the land and oceanic regions the relative magnitude of the two uncertainty measures is strongly dependent upon the number of observing sites and the amount of error they are assigned. This difference is most evident when comparing the tropical regions, where observations are sparse, and the northern extratropical regions where observations are much more common. The within uncertainty is large in the tropical regions compared to the uncertainty due to model spread. Conversely, the within error is relatively small in the northern extratropics compared to the model spread. The increase in model spread in regions with greater observational constraint is largely due to the fact that the differences in model transport are more often quantified where observations exist.

3.2.2. Sensitivity to Prior Flux Uncertainties

[36] One can vary the prior flux uncertainty to further explore the level to which the prior flux is influencing the inversion results. This has been accomplished by increasing the prior flux uncertainties to 2, 5, and 10 times the levels used in the control case inversion. Figure 6a shows the results of this sensitivity test for a few selected regions. Regions for which observations provide constraint show little change as the prior flux uncertainty is increased. However, regions where data is sparse (tropical land and South Atlantic) show considerable sensitivity to the prior uncertainty. This confirms the limited confidence that should be placed on the tropical land and certain ocean regions suggested by the flux uncertainties presented in Figures 3, 4, and 5. Because these regions have very little data constraint, they tend to be constrained by the prior and prior uncertainty level unless required to compensate for changes in those regions with data constraint such as the northern land and many of the ocean regions. This compensation is a direct result of the requirement to maintain the global mass balance defined by the atmospheric growth rate. This is most obvious in the case of the Tropical and South Atlantic Ocean regions where large anti-correlated fluxes observed.

[37] Figure 6a also shows an extreme sensitivity test in which the background biosphere exchange amplitude has been reduced to 50% of that used in the control case in all months. This further confirms the data constraint evident in the northern extratropical regions and the limited confidence that accompany the tropical land and certain ocean regions.

[38] In order to test the possibility that terrestrial seasonality is "leaking" into the estimated fluxes for the northern oceanic regions, the inversion was run with reduced (factor of 4) prior uncertainties for the North Pacific, Northern Ocean, and North Atlantic regions. These ocean regions are then strongly constrained to mimic the prior flux seasonality. Figure 6b shows the resulting fluxes and difference for the summation of the northern land regions (Boreal and Temperate North America, Boreal and Temperate Asia, Europe). As shown in Figure 6b, the suppression of the heightened seasonality for the northern ocean regions is shifted to the adjacent land regions and follows the terrestrial seasonal cycle quite closely. The magnitude of the flux difference is small compared to the northern land seasonal fluxes, so this has little impact on the estimated fluxes for land. Though not conclusive, the result of this test is consistent with leakage of land fluxes into the adjacent ocean regions. Though not performed in the TransCom 3 experiment, inclusion of carbon isotope or O_2/N_2 values would more conclusively test this hypothesis.

3.2.3. Predicted CO_2

[39] Figure 7a shows the difference between the model mean predicted CO_2 concentration and the observed CO_2 at all stations and months. The largest mismatches occur for Hungary (HUN: 16.7°E, 47°N) in winter, which is likely due to the difficulty of matching concentrations at a site with large observed variability not expected to be captured by the global scale transport models used in this study. Fortunately, this station has large "data uncertainty" (1.4 to 4.0 ppm), so models are only weakly required to match the observed concentration. When the mismatches are scaled by their assigned uncertainty, a different picture emerges. This quantity, the station by station contribution to the cost function or "χ^2 per station," is formally expressed as

$$\chi_i^2 = \frac{\left(D_i^s - D_i^o\right)^2}{\sigma_i^2}, \tag{5}$$

where D_i^s is the simulated concentration at station i and D_i^o is the observed concentration at station i with uncertainty σ_i [*Peylin et al.*, 2002]. Values much greater than 1 indicate that the difference between the predicted and observed concentration at that station is much greater than the uncertainty assumed in the inversion. This suggests that the uncertainty assigned to these stations is too small and, hence, they may be influencing the inversion result more than is warranted.

[40] Figure 7b shows the annual mean of these values against station latitude. One station in particular, Cape Rama India (CRI: 73.8°E, 15.1°N) shows an annual mean χ_i^2 value of 3.4, indicating that the mismatch between the

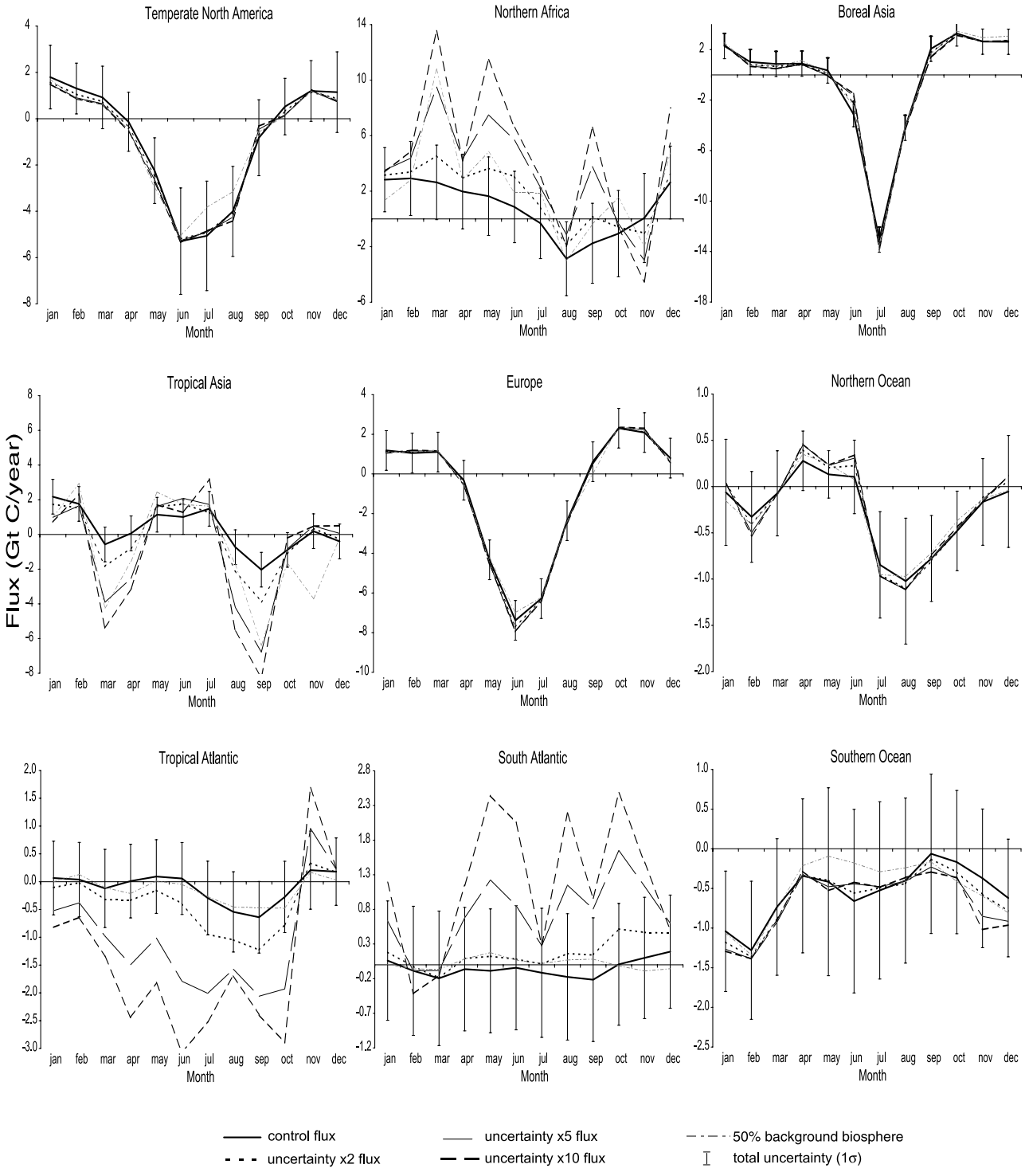

Figure 6a. Model mean control flux, and estimated fluxes with prior uncertainties scaled by factors of 2, 5, and 10 for selected land and ocean regions. Also shown are the results for a case in which the background biosphere exchange is reduced to 50% of that used in the control run. The total uncertainty (between and within uncertainty) for the control case is provided. Note that the vertical scale varies.

predicted and observed CO_2 concentration is almost twice the assigned uncertainty. Upon closer examination, this is primarily due to the χ^2_i value in the month of February (14.7), which is due to a combination of low assigned uncertainty (0.8 ppm) and relatively large mismatches (model mean of 2.8 ppm). Other stations with two or more months exceeding a χ^2_i value of 4 are Guam (GMI: 144.8°E, 13.4°N, December, January, March), Izana,

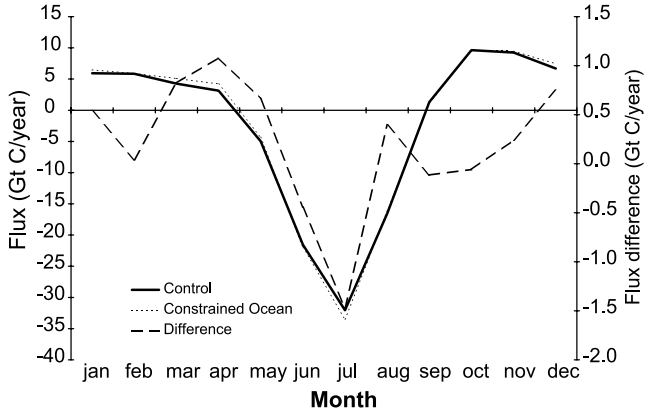

Figure 6b. Estimated fluxes for the control case, the case in which prior uncertainties for the North Pacific, Northern Ocean, and North Atlantic are reduced by a factor of 4, and the difference. The fluxes represent the sum of the Boreal North America, Temperate North America, Boreal Asia, Temperate Asia, and Europe regions.

Canary Islands (IZO: 16.5°W, 28.3°N, June, July), Utah, United States (UTA: 113.7°W, 39.9°N, January, February), Colorado, United States, 5000 m (CARR: 104.8°W, 40.9°N, March, April), Plateau Rosa, Italy (PRS: 7.7°E, 49.3°N, June, July), and Hungary (December, January). Sensitivity tests of the annual mean inversion found simi-lar results for Guam and Cape Rama India [*Law et al.*, 2003].

[41] By the same token, χ_i^2 values much less than one indicate stations for which the assigned uncertainty may be too large and should, therefore, contribute more to the total χ^2 value. Stations for which the annual mean χ_i^2 value is less than 0.25 (indicating mismatches $^1/_2$ the assigned uncertainty) include Bass Strait, Tasmania (AIA: 144.3°E, 40.5°S), South Pole (SPO: 24.8°W, 90°S), Halley Bay, Antarctica (HBA: 25.5°W, 75.7°S), Syowa Station, Antarctica (SYO: 39.6°E, 69°S), Mawson Station, Antarctica (MAA: 62.9°W, 67.6°S), and Palmer Station, Antarctica (PSA: 64°W, 64.9°S). All of these stations are in the southern high latitudes.

[42] In order to confirm that these stations are either providing too much or too little weight to the inversion, a number of tests have been performed. In the first, the stations with large χ_i^2 values are removed from the inversion. In the second, the stations with small χ_i^2 values are adjusted such that their uncertainty is reduced by a factor of 2. In the last test, both of these changes are made. The results are shown in Figure 8. The tropical regions show the most significant changes, and independent tests (not shown) indicate that these are due primarily to the removal of the Guam and Cape Rama India stations. Reduction of the uncertainty associated with the southern high latitude stations had a negligible impact on the regional fluxes except for some small changes in the South Indian Ocean region.

[43] Given the much greater number of observing sites over the northern extratropics, the removal of a few sites has little impact on the fluxes in those regions. However, the removal of Guam and Cape Rama, India, constitute a considerable reduction in observational constraint in the tropics and hence, lead to changes in those regions primarily.

4. Discussion

4.1. Comparison to Annual Mean Inversion

[44] Table 1 presents the model mean, annual mean carbon flux estimates for each of the land and ocean regions considered in this study. In addition, the model mean flux estimates from the previously published annual mean inversion are included for comparison. The two studies show considerable agreement in all regions with the exception of Northern Africa. The current study estimates an annual mean release from this region (0.79 ± 1.0 Gt C/year) compared to the previous study which estimated no net flux (0.01 ± 1.3 Gt C/year). However, given the large amount of uncertainty associated with the estimates for this region, the change lies within the uncertainty. Since the global total atmospheric growth rate is identical in the two studies, the difference in Northern Africa must be compensated for elsewhere. This occurs equally across the Tropical Asia and Australasia regions, both of which are also estimated with considerable uncertainty. Examination of the aggregated land and ocean totals indicates that the differences between the two studies reflect compensatory fluxes between the Tropical and Southern land and ocean regions, respectively.

[45] In the northern extratropical regions, the current study estimates a slightly larger annual mean net uptake in Europe but produces less uptake in Temperate and Boreal Asia. However, each of these differences is well within the estimated uncertainty.

[46] The consistency between the annual mean inversion and the annual mean calculated from the seasonal inversion is consistent with a recent study exploring various aspects of the CO_2 inversion problem [*Peylin et al.*, 2002]. In their 17-region inversion, which studied results from three models, the authors found regional model mean differences no larger than 0.5 Gt C/year.

4.2. Posterior Flux Amplitude

[47] As suggested in section 3.1, the posterior flux seasonality for the northern land, in particular, will reflect adjustments to the background responses such that the total predicted CO_2 seasonal cycle best matches the observed CO_2 seasonal cycle. Figure 9a ($r^2 = 0.7$) shows the model-specific relationship between the estimated northern land flux amplitude and the northern extratropical background concentration amplitude (the values in Figure 2 legend). As expected, those models which generated relatively weak seasonality when driven by the background fluxes (UCI, JMA, TM2, UCB), generate estimated northern land flux amplitudes that are generally the largest among the 12 models. Models which generated strong seasonality in response to the background fluxes (MATCH:NCEP, NIRE, TM3, GCTM) require less seasonal adjustment in order to match the CO_2 observations over the northern extratropics.

[48] A similar relationship is evident when these indices are considered in conjunction with the annual mean estimated northern land flux. Figure 9b ($r^2 = 0.6$) shows the model-specific relationship between the northern extratropical background concentration amplitude and the estimated

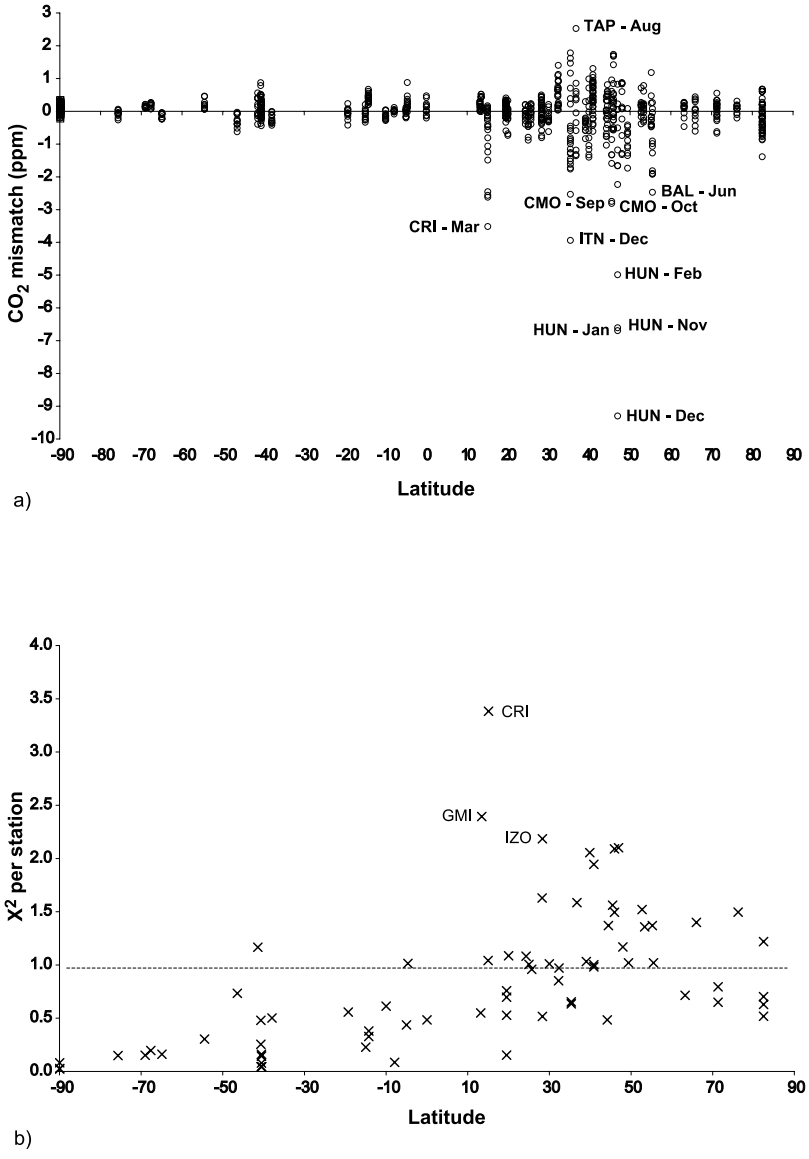

Figure 7. (a) Difference between the model mean predicted CO_2 concentration and the observed. The model mean dramatically underestimates winter concentrations at Hungary. (b) Model/Annual mean of the χ^2 per station values. Largest values are noted for Cape Rama India (CRI), Guam (GMI), and Izana Observatory (IZO).

annual mean northern land flux. Most of the models which generated weak seasonality in response to the background fluxes (UCI, JMA, TM2) and required more seasonal flux adjustment also infer the smallest annual mean uptake in the northern land regions. The relationships exhibit some scatter. For example, UCB which was one of the models with a weak background response amplitude requires a relatively large northern land sink. This may be due to the strong background response to winter emissions but a relatively weak response to summer uptake (see Figure 1a).

[49] In previous work, the annual mean northern land flux correlated with the strength of the model rectifier and the distribution of the models follows closely the distribution found in Figure 9 [*Gurney et al.*, 2003]. Hence models which respond vigorously to the background fluxes, simulate strong annual mean rectifiers, require less seasonal flux adjustment and require the largest northern land sink to best match observed CO_2.

4.3. Mechanistic Implications of the Inverse Estimates

[50] Consistent with a variety of other studies, a large northern extratropical land sink (-2.5 ± 1.2 Gt C/year) is evident in the results presented here [*Tans et al.*, 1990; *Ciais et al.*, 1995; *Fan et al.*, 1998; *Bousquet et al.*, 1999; *Kaminski et al.*, 1999; *Pacala et al.*, 2001; *Baker*, 2001; *Peylin et al.*, 2002]. Our annual mean uptake is greater in Temperate North America (-0.90 ± 0.5 Gt C/year) and Europe (-0.98 ± 0.4 Gt C/year), with less uptake in Temperate Asia (-0.43 ± 0.7 Gt C/year) and Boreal Asia (-0.39 ± 0.7 Gt C/year). A number of different hypotheses

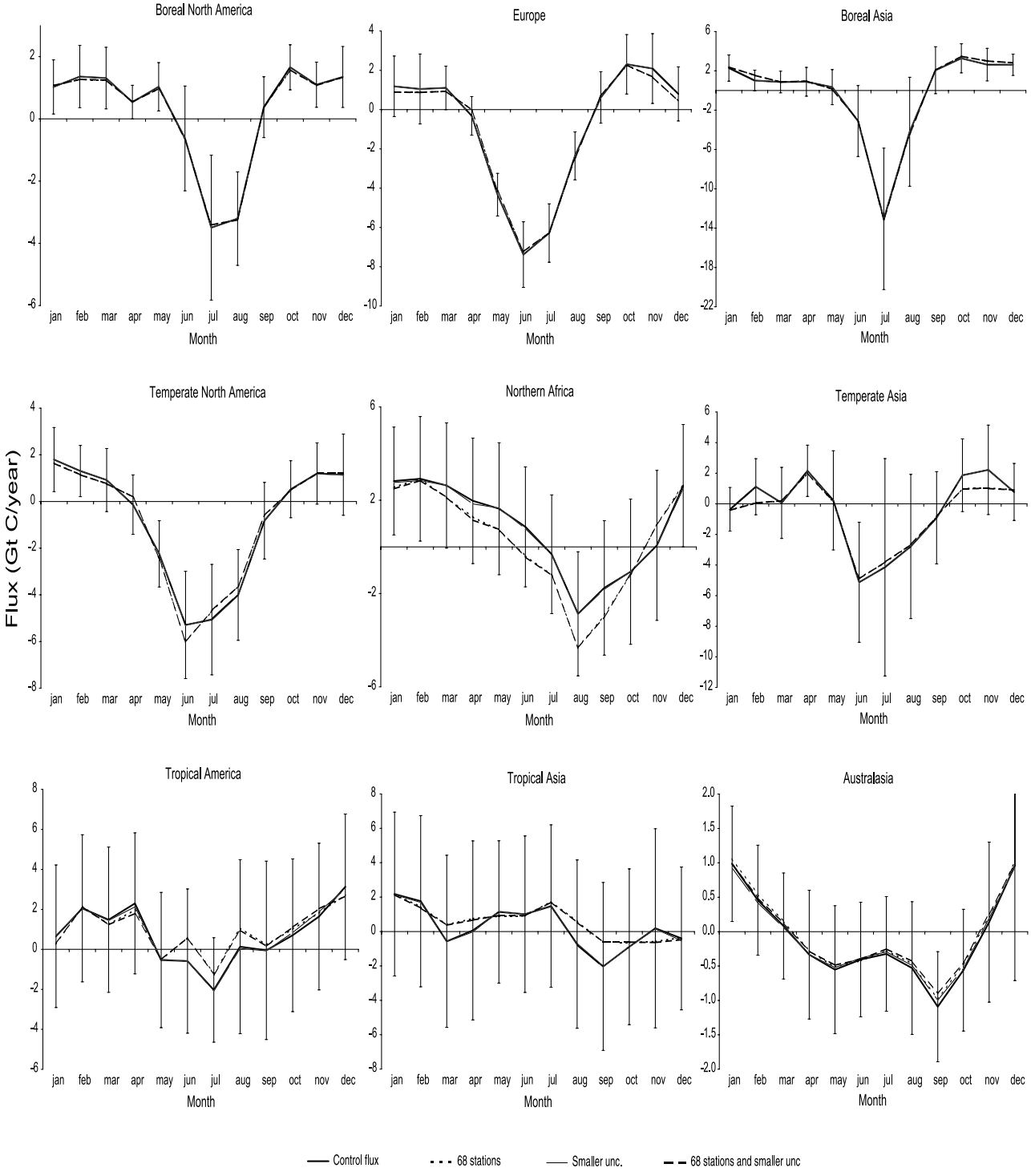

Figure 8a. Station sensitivity for selected land regions. Estimated flux for the control inversion (75 stations), an inversion with 68 stations (removed CRI, GMI, IZO, UTA, Carr 5000m, PRS, and HUN), the control inversion with halved uncertainty on six southern stations (Bass Strait, SPO, HBA, SYO, MAA, and PSA), and an inversion with the combination of these two station adjustments. Note that the vertical scale varies. The fluxes do not include fossil fuel emissions.

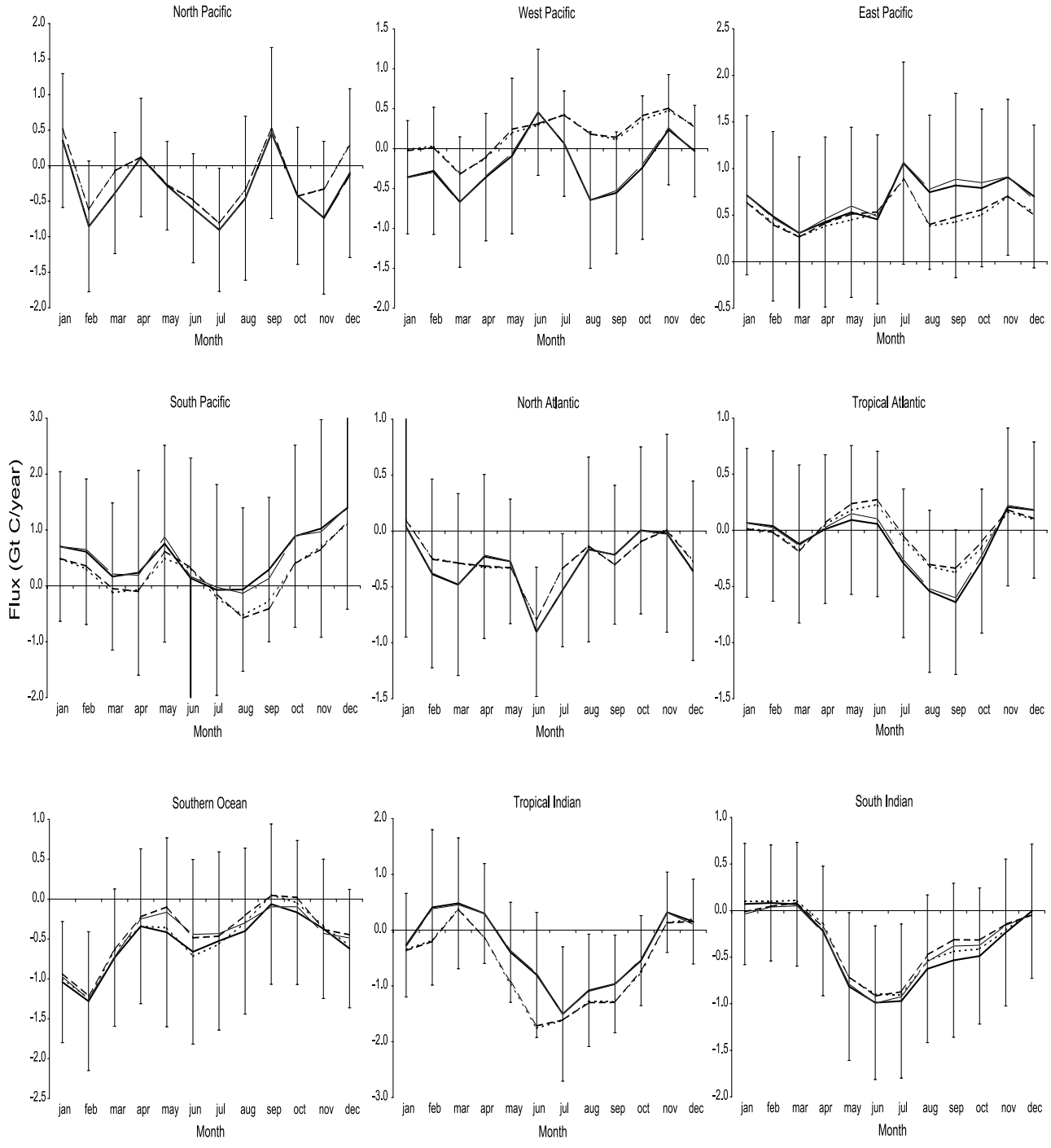

Figure 8b. As in Figure 8a but for selected ocean regions.

have been proffered to explain this residual uptake. These include fertilization by Nitrogen or CO_2 itself, changes in temperature and precipitation, and alterations in land-use [*Houghton et al.*, 1998; *Schimel et al.*, 1996; *Prentice et al.*, 2001]. Though the flux estimates in Figures 3, 4, and 5 cannot explicitly test these hypotheses, the broad features in the northern land regions may provide some useful additions to the current evidence supporting the various proposed uptake mechanisms. Both Boreal Asia and Europe show greater uptake or lessened respiration at the height of the growing season when compared to the seasonally balanced prior flux. Even when additional uptake as estimated by inventory studies is included, the peak European uptake is significantly greater than the prior flux. One possible explanation of this is the use of air temperature rather than soil temperature in the CASA model used to generate the prior flux estimates. This would tend to increase the level of heterotrophic respiration and hence offset the net uptake over the growing season. This is further suggested by the difference in many of these

Table 1. Annual Model Mean Flux Estimates, Uncertainties, and Results From Previously Published Annual Mean Inversion Study

Region	Mean Estimated Flux, Gt C/year	"Within" Uncertainty, Gt C/year	"Between" Uncertainty, Gt C/year	*Gurney et al.* [2002] Inversion,[a] Gt C/year	Flux Difference, Gt C/year
Boreal North America	0.20	0.18	0.28	0.28	−0.08
Temperate North America	−0.89	0.22	0.32	−0.82	−0.07
Tropical America	0.74	0.73	0.77	0.67	0.07
South America	−0.24	0.64	0.61	−0.12	−0.12
Northern Africa	0.79	0.54	0.85	−0.01	0.78
Southern Africa	−0.51	0.58	0.60	−0.29	−0.22
Boreal Asia	−0.36	0.23	0.51	−0.60	0.23
Temperate Asia	−0.41	0.34	0.74	−0.42	0.01
Tropical Asia	0.27	0.45	0.94	0.42	−0.15
Australasia	−0.10	0.14	0.15	−0.15	0.05
Europe	−0.96	0.18	0.43	−0.61	−0.35
North Pacific	−0.32	0.14	0.28	−0.25	−0.06
West Pacific	−0.21	0.15	0.27	−0.15	−0.05
East Pacific	0.66	0.18	0.27	0.63	0.03
South Pacific	0.51	0.29	0.49	0.49	0.01
Northern Ocean	−0.27	0.08	0.17	−0.30	0.02
North Atlantic	−0.29	0.15	0.30	−0.45	0.16
Tropical Atlantic	−0.10	0.18	0.16	−0.05	−0.05
South Atlantic	−0.05	0.24	0.07	−0.04	−0.01
Southern Ocean	−0.55	0.17	0.33	−0.47	−0.08
Tropical Indian Ocean	−0.33	0.19	0.26	−0.34	−0.01
South Indian Ocean	−0.39	0.19	0.22	−0.24	−0.15
Northern land	−2.42	0.30	1.09	−2.16	−0.26
Tropical land	1.80	0.78	1.65	1.10	0.70
Southern land	−0.85	0.70	0.94	−0.56	−0.29
Northern ocean	−0.88	0.24	0.51	−1.00	0.12
Tropical ocean	0.03	0.37	0.41	0.09	−0.06
South ocean	−0.49	0.39	0.51	−0.26	−0.22
Total Land	−1.46	0.62	0.75	−1.62	0.16
Total Ocean	−1.34	0.62	0.75	−1.18	−0.16
Global Total	−2.81	0.01	0.001	−2.80	−0.01

[a]This reflects an annual mean inversion without the Darwin observing station.

northern land regions during the winter. Europe, Boreal Asia, Temperate North America, and Temperate Asia all contain months where the estimated flux is lower than the prior value, suggesting less winter respiration than the prior model. Differences in peak growing season uptake could also be due to errors in the NPP estimated in the prior model which are primarily driven by NDVI measurements [*Potter et al.*, 1993]. This is also relevant for the considerable mismatch of peak uptake in the Temperate Asian region. Many of the models in this study place the maximum uptake in June, whereas the prior model placed the maximum in August. This difference in peak uptake suggests that the June CO_2 concentration, driven primarily by the background biosphere exchange, is too high relative to observations and hence a large sink is required to reduce this mismatch.

[51] Because the Temperate Asian region spans latitudes from roughly 15°N to 45°N and has only a few CO_2 observing sites, the difference may be due to poor regional representation in the inverse estimate [*Kaminski et al.*, 2001; *Engelen et al.*, 2002]. Such "representation error" is further suggested by performing the inversion without the Ulann Uul Mongolia (UUM: 111.10°E, 44.5°N), Tae-ahn Peninsula (TAP: 126.13°E, 36.73°N), and Ryori Japan (RYO: 141.83°E, 39.03°N) CO_2 observing stations. Removal of these stations results in a more even distribution of uptake across the June to August timeframe. The seasonality of these three influential stations within and downwind of the Temperate Asian region are likely not representative of the region as a whole. Hence the background biospheric exchange generates CO_2 levels that reflect the whole region while the inverted fluxes are driven by a small spatially biased sample of atmospheric CO_2 as measured by these influential stations. Subdivision of the Temperate Asia region may result in a less biased posterior flux estimate but would likely increase the posterior uncertainty. The motivation for limiting the number of inverted regions is the reduction of random error and the need to limit the computation burden of the forward model simulations. This trade-off between random error and bias is further discussed in recent work [*Baker*, 2001].

[52] This source of error in the inversion set-up itself is one source of potential bias that is very likely present in undersampled regions. The other primary source of error in the inversion approach is error due to transport. TransCom was initially devised to explore that magnitude of the transport error. However, only the random component (the between uncertainty estimates) can be quantified here. In considering the model mean flux estimates, this error may be minimized through the use of the model average. However, all models may contain the same transport biases and therefore result in biased flux estimates.

[53] Both the boreal regions show a slight delay in the onset of growing season uptake relative to the prior model. As

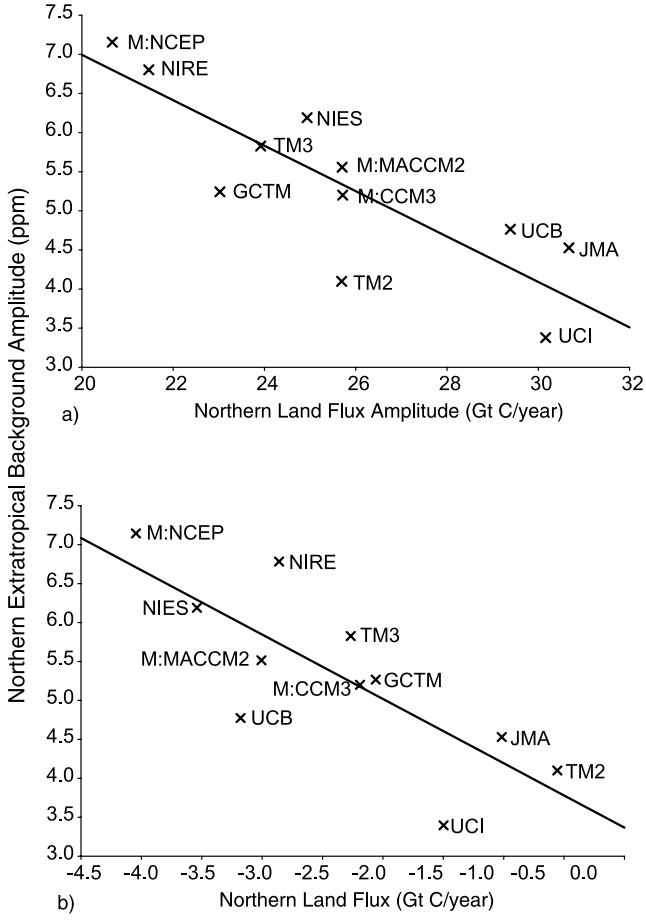

Figure 9. (a) Estimated Northern land flux amplitude (October through March minus June through August) versus the northern extratropical background (fossil plus neutral bio plus background ocean) response amplitude (r^2 = 0.75). (b) Northern land flux versus the northern extratropical background response amplitude (r^2 = 0.62).

suggested by other work, this may be the result of earlier Spring thaw, resulting in an imbalance of respiration over photosynthesis [*Goulden et al.*, 1998]. In the month of June, this would require a 50% and 38% increase in the prior model respiration flux in order to match the estimated flux for the Boreal North American and Boreal Asian regions, respectively.

5. Conclusions

[54] With the participation of 12 atmospheric tracer transport models, a control case has been constructed to characterize the seasonal sources and sinks of carbon as another step in the TransCom atmospheric CO_2 inversion experiment. In order to construct this control inversion, decisions regarding prior fluxes, flux uncertainties, observational data and observational data uncertainties have been made.

[55] As found in recent TransCom work, the model responses to the background tracers provide a first indication of model to model differences. In the current experiment, the amplitude of the background flux response was inversely related to the amplitude of the estimated northern land flux. Furthermore, those models that exhibit a weak response amplitude to the background flux are among the models with the smallest northern land sink. This relationship is consistent with earlier TransCom results showing the relationship between models that tend to rectify seasonal exchange with the biosphere and the annual mean estimated net uptake over the northern land.

[56] For the northern land regions, the model mean results show deviations from the prior flux in both the growing season and during winter months. Most notable are the significantly greater uptake during the height of the growing season over Europe compared to the prior model. Temperate North America and Boreal Asia exhibit less emission during some winter months, while a 2-month discrepancy exists regarding the timing of peak uptake in Temperate Asia.

[57] The northern oceans show heightened seasonality that may be due to misallocation of terrestrial flux to adjacent oceanic regions. As with the earlier annual mean inversion results, the Southern Ocean region exhibits less carbon uptake than ΔpCO_2 measurements would suggest. There is general agreement between the ΔpCO_2-based prior flux and the fluxes estimated here for Austral summer, but significant departures during fall and spring months occur suggesting that the timing of ΔpCO_2 observations may be, in part, responsible for the discrepancy.

[58] Owing to limited CO_2 observations, tropical regions, particularly over land, show considerable uncertainty and may contain unrealistic seasonal swings in flux due to unconstrained adjustments to maintain the global mass balance constraint. These regions are far more sensitive to prior flux uncertainties than the northern extratropics which show insensitivity to this aspect of the inversion set-up.

[59] The timing of the differences between the prior model and the estimated fluxes suggest that respiration may play an important role in either errors in the prior model or real changes in the winter flux for the northern extratropical land regions. In particular, changes in the timing of increased springtime respiration versus photosynthesis may explain the lessened net spring uptake in Boreal North America and Boreal Asia.

[60] Biases caused by transport error across all models or representation error are potential limitations to this method. However, only random errors are characterized in this study. Furthermore, interpretation is somewhat limited by examination of a single 5-year mean and the use of the single station network used here. Though we have tested the model mean inversion result to some aspects of the inversion set-up, this is not exhaustive, and future work will test further elements, in particular those related to station choices and uncertainties. Finally, interannual variations in seasonality, which may give further mechanistic insight, have not been explored in this study.

[61] Further results from the TransCom experiment are forthcoming. In particular, results are expected from an interannual inversion, model to model comparisons, and a comparison of inverse results using different inversion approaches. These constitute the last primary elements of the TransCom 3 intercomparison and should shed further

light on the sources and sinks of carbon and the sources of uncertainty in making these inverse estimates.

[62] **Acknowledgments.** This work was made possible through support from the National Science Foundation (OCE-9900310), the National Oceanic and Atmospheric Administration (NA67RJ0152, Amend 30), and the International Geosphere Biosphere Program/Global Analysis, Interpretation, and Modeling Project. S. Fan and J. Sarmiento acknowledge support from NOAA's Office of Global Programs for the Carbon Modeling Consortium.

References

Andres, R. J., G. Marland, I. Fung, and E. Matthews (1996), A 1° × 1° distribution of carbon dioxide emissions from fossil fuel consumption and cement manufacture, 1950–1990, *Global Biogeochem. Cycles*, *10*(3), 419–429.

Baker, D. F. (2001), Sources and sinks of atmospheric CO_2 estimated from batch least-squares inversions of CO_2 concentration measurements, Ph.D. dissertation, Princeton Univ., Princeton, N. J.

Bousquet, P., P. Ciais, P. Peylin, M. Ramonet, and P. Monfrey (1999), Inverse modeling of annual atmospheric CO_2 sources and sinks: 1. Method and control inversion, *J. Geophys. Res.*, *104*(D21), 26,161–26,178.

Bousquet, P., P. Peylin, P. Ciais, C. Le Quéré, P. Friedlingstein, and P. Tans (2000), Regional changes in carbon dioxide fluxes of land and oceans since 1980, *Science*, *290*, 1342–1346.

Ciais, P., P. P. Tans, M. Troliier, J. W. C. White, and R. J. Francey (1995), A large Northern Hemisphere terrestrial CO_2 sink indicated by the $^{13}C/^{12}C$ ratio of atmospheric CO_2, *Science*, *269*, 1098–1102.

Denning, A. S., M. Holzer, K. R. Gurney, M. Heimann, R. M. Law, P. J. Rayner, I. Y. Fung, S. Fan, S. Taguchi, P. Friedlingstein, Y. Balkanski, J. Taylor, M. Maiss, and I. Levin (1999), Three-dimensional transport and concentration of SF6: A model intercomparison study (TransCom 2), *Tellus, Ser. B*, *51*, 266–297.

Engelen, R. J., A. S. Denning, and K. R. Gurney (2002), On error estimation in atmospheric CO_2 inversions, *J. Geophys. Res.*, *107*(D22), 4635, doi:10.1029/2002JD002195.

Enting, I. (2002), *Inverse Problems in Atmospheric Constituent Transport*, Cambridge Univ. Press, New York.

Enting, I. G., C. M. Trudinger, and R. J. Francey (1995), A synthesis inversion of the concentration and $\delta^{13}C$ of atmospheric CO_2, *Tellus, Ser. B*, *47*, 35–52.

Fan, S., M. Gloor, J. Mahlman, S. Pacala, J. Sarmiento, T. Takahashi, and P. Tans (1998), A large terrestrial carbon sink in North America implied by atmospheric and oceanic carbon dioxide data and models, *Science*, *282*, 442–446.

GLOBALVIEW-CO_2 (2000), Cooperative Atmospheric Data Integration Project—Carbon Dioxide [CD-ROM], NOAA Clim. Model. and Diag. Lab., Boulder, Colo.

Goulden, M. L., et al. (1998), Sensitivity of boreal forest carbon balance to soil thaw, *Science*, *279*, 214–217.

Gurney, K., R. Law, P. Rayner, and A. S. Denning (2000), TransCom 3 experimental protocol, Pap. 707, Dept. of Atmos. Sci., Colo. State Univ. (Available at http://transcom.colostate.edu/TransCom_3/transcom_3.html)

Gurney, K. R., et al. (2002), Towards robust regional estimates of CO_2 sources and sinks using atmospheric transport models, *Nature*, *415*, 626–630.

Gurney, K. R., et al. (2003), Transcom 3 CO_2 Inversion Intercomparison: 1. Annual mean control results and sensitivity to transport and prior flux information, *Tellus, Ser. B*, *55*, 555–579.

Houghton, R. A., E. A. Davidson, and G. M. Woodwell (1998), Missing sinks, feedbacks, and understanding the role of terrestrial ecosystems in the global carbon balance, *Global Biogeochem. Cycles*, *12*(1), 25–34.

Kaminski, T., M. Heimann, and R. Giering (1999), A coarse grid three-dimensional global inverse model of the atmospheric transport: 2. Inversion of the transport of CO_2 in the 1980s, *J. Geophys. Res.*, *104*(D15), 18,555–18,581.

Kaminski, T., P. J. Rayner, M. Heimann, and I. G. Enting (2001), On aggregation errors in atmospheric transport inversion, *J. Geophys. Res.*, *106*(D5), 4703–4715.

Law, R. M., et al. (1996), tions in modeled atmospheric transport of carbon dioxide and the consequences for CO_2 inversions, *Global Biogeochem. Cycles*, *10*(4), 783–796.

Law, R. M., Y.-H. Chen, K. R. Gurney, and TransCom 3 modelers (2003), TransCom 3 CO_2 inversion intercomparison: 2. Sensitivity of annual mean results to data choices, *Tellus, Ser. B*, *55*, 580–595.

Metzl, N., C. Brunet, A. Jabaud-Jan, A. Poisson, and B. Schauer (2001), Summer and winter air-sea CO_2 fluxes in the Southern Ocean, paper presented at Sixth International Carbon Dioxide Conference, Organizing Comm. of 6th Int. Carbon Dioxide Conf., Sendai, Japan.

Pacala, S. W., et al. (2001), Convergence of land- and atmosphere-based U.S. carbon sink estimates, *Science*, *292*, 2316–2320.

Peylin, P., D. Baker, J. Sarmiento, P. Ciais, and P. Bousquet (2002), Influence of transport uncertainty on annual mean and seasonal inversions of atmospheric CO_2 data, *J. Geophys. Res.*, *107*(D19),4385, doi:10.1029/2001JD000857.

Potter, C. S., J. T. Randerson, C. B. Field, P. A. Matson, P. M. Vitousek, H. A. Mooney, and S. A. Klooster (1993), Terrestrial ecosystem production: A process model based on global satellite and surface data, *Global Biogeochem. Cycles*, *7*(4), 811–841.

Prentice, I. C., G. Farquhar, M. Fashm, M. Goulden, M. Heimann, V. Jaramillo, H. Kheshgi, C. Le Quéré, and R. J. Scholes (2001), The carbon cycle and atmospheric carbon dioxide, in *Climate Change 2001: The Scientific Basis, Contribution of Working Group I to the Third Assessment Report of the Intergovernmental Panel on Climate Change*, edited by J. T. Houghton et al., pp. 183–237, Cambridge Univ. Press, New York.

Randerson, J. T., M. V. Thompson, T. J. Conway, I. Y. Fung, and C. B. Field (1997), The contribution of terrestrial sources and sinks to trends in the seasonal cycle of atmospheric carbon dioxide, *Global Biogeochem. Cycles*, *11*, 535–560.

Rayner, P. J., I. G. Enting, R. J. Francey, and R. L. Langenfelds (1999), Reconstructing the recent carbon cycle from atmospheric CO_2, $\delta^{13}C$ and O_2/N_2 observations, *Tellus, Ser. B*, *51*, 213–232.

Rödenbeck, C., S. Houweling, M. Gloor, and M. Heimann (2003), Time-dependent atmospheric CO_2 inversions based on interannually varying tracer transport, *Tellus, Ser. B*, *55*, 488–497.

Schimel, D., D. Alves, I. Enting, M. Heimann, F. Joos, D. Raynaud, and T. Wigley (1996), CO_2 and the carbon cycle, in *Climate Change 1995: The Science of Climate Change*, *Contribution of WG1 to the Second Assessment Report of the IPCC*, edited by J. T. Houghton et al., pp. 65–86, Cambridge Univ. Press, New York.

Takahashi, T., R. H. Wanninkhof, R. A. Feely, R. F. Weiss, D. W. Chipman, N. Bates, J. Olafsson, C. Sabine, and S. C. Sutherland (1999). Net sea-air CO_2 flux over the global oceans: An improved estimate based on the sea–air pCO_2 difference, paper presented at 2nd CO_2 in Oceans Symposium, Cent. for Global Environ. Res. Natl. Inst. for Environ. Stud., Tsukuba, Japan.

Tans, P. P., I. Y. Fung, and T. Takahashi (1990), Observational constraints on the global atmospheric CO_2 budget, *Science*, *247*, 1431–1438.

Tarantola, A. (1987), The least-squares (12-norm) criterion, in *Inverse Problem Theory: Methods for Data Fitting and Parameter Estimation*, chap. 4, pp. 187–287, Elsevier Sci., New York.

D. Baker, National Center for Atmospheric Research (NCAR), Boulder, CO 80303, USA.

P. Bousquet, P. Ciais, and P. Peylin, Laboratoire des Sciences du Climat et de l'Environment (LSCE), F-91198 Gif-sur-Yvette Cedex, France.

L. Bruhwiler, National Oceanic and Atmospheric Administration (NOAA), Climate Monitoring and Diagnostics Laboratory, 326 Broadway R/CG1, Boulder, CO 80303, USA.

Y.-H. Chen, Department of Earth, Atmospheric, and Planetary Science, Massachusetts Institute of Technology (MIT), Cambridge, MA 02141, USA.

S. Denning and K. R. Gurney, Department of Atmospheric Science, Colorado State University, Fort Collins, CO 80523, USA. (denning@atmos.colostate.edu; keving@atmos.colostate.edu)

I. Y. Fung and J. John, Center for Atmospheric Sciences, McCone Hall, University of California, Berkeley, Berkeley, CA 94720-4767, USA.

M. Heimann, Max-Planck-Institute fur Biogeochemie, D-07701 Jena, Germany.

R. Law and P. Rayner, CSIRO Atmospheric Research, PMB 1, Aspendale, Victoria 3165, Australia. (rachel.law@csiro.au; peter.rayner@csiro.au)

T. Maki, Quality Assurance Section, Atmospheric Environment Division, Observations Department, Japan Meteorological Agency, 1-3-4 Otemachi, Chiyoda-ku, Tokyo 100-8122, Japan.

S. Maksyutov, Institute for Global Change Research, Frontier Research System for Global Change, Yokohama 236-0001, Japan.

B. C. Pak and M. Prather, Earth System Science, University of California, Irvine, CA 92697-3100, USA. (bpak@halo.ps.uci.edu)

S. Taguchi, National Institute of Advanced Industrial Science and Technology, 16-1 Onogawa Tsukuba, Ibaraki 305-8569, Japan.

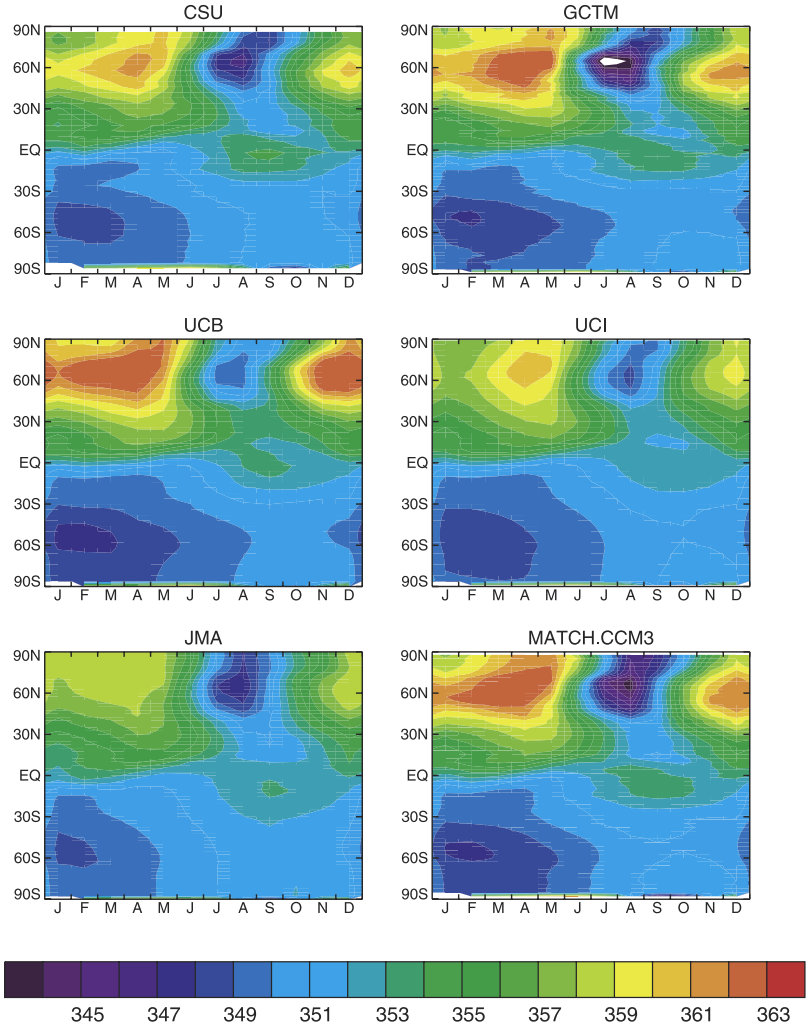

Figure 1. Zonal mean monthly predicted concentration driven by the background fluxes (fossil fuel, seasonally balanced biosphere exchange, ocean exchange) for each of the participating tracer transport models.

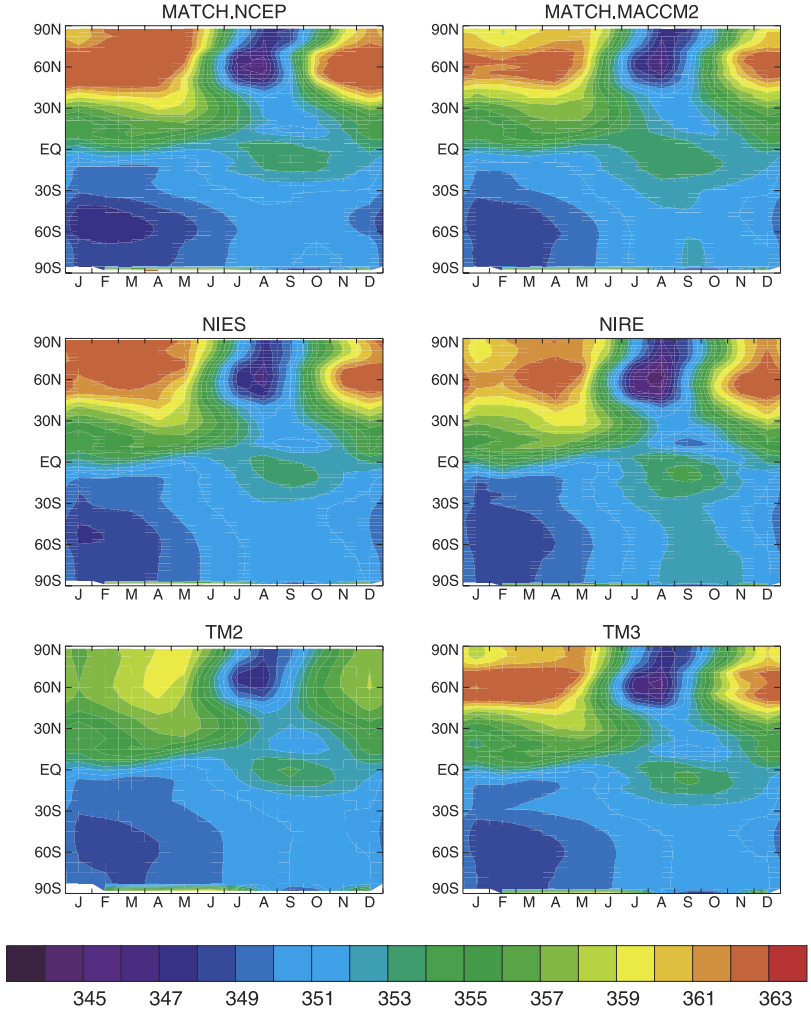

Figure 1. (continued)

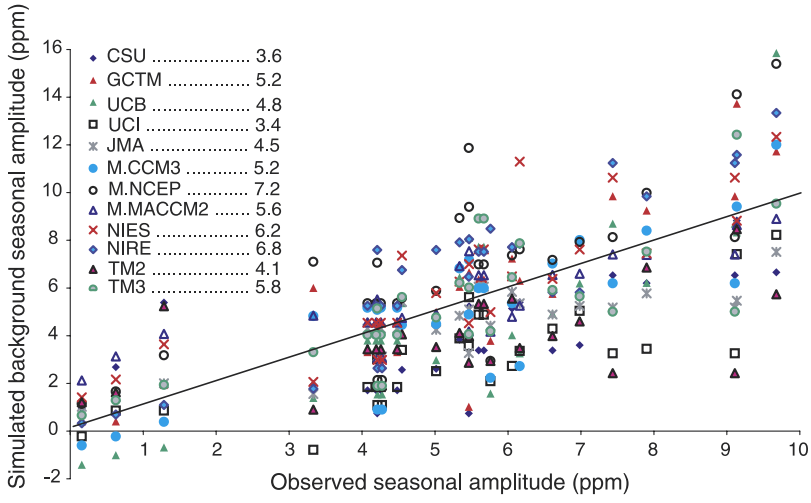

Figure 2. Simulated background seasonal amplitude versus the observed amplitude at stations north of 35°N. Amplitude is defined as the mean October–March concentration minus the mean June–August concentration. The station average simulated values are provided in the legend. The observed station average is 5.6 ppm. A one-to-one line is included.